*J. Fluid Mech.* (1984), *vol.* 147, *pp.* 353–371
*Printed in Great Britain*



# Reynolds-stress measurements in a turbulent trailing vortex

By W. R. C. PHILLIPS† AND J. A. H. GRAHAM‡
Department of Mechanical Engineering, McGill University, Quebec, Canada

(Received 26 October 1983 and in revised form 12 April 1984)

Measurements of a turbulent trailing vortex in zero pressure gradient are described. These include mean velocities and all the components of the Reynolds-stress tensor. The measurements were made using linearized hot wires at stations 45, 78 and 109 chordlengths downstream of the wing. Axisymmetric jets or wakes were added coaxially to the vortex while the total circulation was held constant, and their effect studied. It was found, as Poppleton and Mason & Marchman have reported, that increasing the flow force hastens the radial dispersion of vorticity; this is seen to be concurrent with higher turbulence intensities and Reynolds shear stresses. With the flux of excess axial momentum effectively zero, thereby approximating a turbulent line vortex, no discernible downstream change was observed in the velocity field and very little in the turbulence field.

A balance of terms in the mean-momentum equations is presented and discussed. It is seen that, in spite of the fact that the radial velocity is numerically much smaller than the axial velocity, terms that contain it, both in the axial- and tangential-momentum equations, cannot be ignored, unless the magnitude of the flow force (divided by the fluid density) is much less than the square of the total circulation.

## 1. Introduction

The present article is concerned with an experimental investigation of a turbulent trailing vortex, and in particular one with superimposed coaxial jets or wakes. Such studies are not new, but, possibly because of the danger trailing vortices pose to other aircraft, the primary aim of much, though not all, experimental work to date has been to help in developing empirical methods to predict the evolution of the vortex, or in devising methods to rapidly dissipate its vorticity (see e.g. Poppleton 1971*a*; Corsiglia & Dunham 1976; Smith 1980). The only detailed turbulence measurements would appear to be those of Poppleton (1971*b*) and Singh (1974).

Poppleton imposed jets of varying momentum on to a vortex generated by a differential aerofoil and measured all components of the Reynolds-stress tensor and velocity vector at three downstream stations. Singh was concerned with laminar instabilities in an isolated trailing vortex, and studied the vortex trailing from a highly loaded single aerofoil. He measured some components of the Reynolds stress tensor, in addition to the axial and tangential velocities, at four downstream stations.

Knowledge of the turbulence field is useful not only in helping to acquire clear ideas about the vortex structure, but also in developing a general understanding of the behaviour of turbulent flows with significant mean-streamline curvature, and for turbulence modellers as a test case. Since Poppleton's results contain much scatter

† Present address: University of Melbourne, Parkville, Victoria 3052, Australia.
‡ Present address: Canadian Pratt & Whitney Co., Longueuil, Quebec, Canada.

and Singh's are incomplete, the aim of the present work was to obtain such measurements with a view to providing more definitive data than has hitherto been available.

Acquiring such measurements in a vortex trailing from a single aerofoil is not without its difficulties, however, since the vortex will move owing to the presence of a probe (Mason & Marchman 1972), and is prone to wander (Baker *et al.* 1974). A less sensitive vortex is that which forms and trails from two identical aerofoils radial to an axis of symmetry and each inclined at the same angle of attack (as viewed from the axis of symmetry). Hoffmann & Joubert (1963) found such an arrangement produced 'a stable single vortex. . . whose position in the tunnel remained almost completely independent of velocity, angle of attack and downstream distance'; and the insertion of a probe (Poppleton). In consequence we generate our vortex with a similar arrangement.

Five flows are studied: in two a jet is superimposed coaxially with the vortex; a further two have a coaxial wake, while the fifth approximates a turbulent line vortex. In each we use linearized hot wires to measure the velocity vector and all components of the Reynolds-stress tensor at 45, 78 and 109 chordlengths downstream of the wing. The free-stream velocity was low enough to consider the flow incompressible and yielded a Reynolds number, based upon wing chord, of about $7.4 \times 10^4$.

A preliminary report on this work, and some of the data (plus an empirical theory), was presented at a meeting of the International Council of the Aeronautical Sciences (Graham, Newman & Phillips 1974); while the complete set of data is given in Graham & Phillips (1975).

## 2. Governing equations

We use cylindrical coordinates $(cr, \theta, cz)$ with $z$ in the streamwise direction. The corresponding mean velocity components are $(Uv_r, Uv_\theta, Uv_z)$. Then the mean momentum equations for steady axisymmetric flow are, without approximation,

$$\frac{\partial}{\partial z}(v_r v_z + \overline{v_r' v_z'}) = -\frac{\partial p}{\partial r} + Re^{-1}\left\{\frac{\partial}{\partial r}\left(\frac{1}{r}\frac{\partial}{\partial r}(rv_r)\right) + \frac{\partial^2 v_r}{\partial z^2}\right\} - \frac{1}{r}\frac{\partial}{\partial r}(rv_r^2 + r\overline{v_r'^2}) + \frac{1}{r}(v_\theta^2 + \overline{v_\theta'^2}), \tag{1}$$

$$\frac{\partial}{\partial z}(v_z v_\theta + \overline{v_z' v_\theta'}) = Re^{-1}\left\{\frac{1}{r^2}\frac{\partial}{\partial r}\left(r^3\frac{\partial}{\partial r}\left(\frac{v_\theta}{r}\right)\right) + \frac{\partial^2 v_\theta}{\partial z^2}\right\} - \frac{1}{r^2}\frac{\partial}{\partial r}(r^2 v_r v_\theta + r^2\overline{v_r' v_\theta'}), \tag{2}$$

$$\frac{\partial}{\partial z}(v_z^2 + \overline{v_z'^2} + p) = Re^{-1}\left\{\frac{1}{r}\frac{\partial}{\partial r}\left(r\frac{\partial v_z}{\partial r}\right) + \frac{\partial^2 v_z}{\partial z^2}\right\} - \frac{1}{r}\frac{\partial}{\partial r}(rv_r v_z + r\overline{v_r' v_z'}). \tag{3}$$

And the equation of mass conservation is given by

$$\frac{1}{r}\frac{\partial r v_r}{\partial r} + \frac{\partial v_z}{\partial z} = 0. \tag{4}$$

Here the wing chord is $c$, the free-stream velocity $U$, the pressure $p\rho U^2$, and Reynolds number $Re = Uc/\nu$.

With constant $U$, the integral relations for a fully rolled-up trailing vortex are, from (2) and (4), provided that $r^2\overline{v_r' v_\theta'} \to 0$ as $r \to \infty$,

$$\int_0^\infty \{(\Gamma - \Gamma_0) v_z + 2\pi r\overline{v_\theta' v_z'}\} r\,\mathrm{d}r = -2\,Re^{-1}\Gamma_0 z + \text{const}, \tag{5}$$

where $\Gamma = 2\pi r v_\theta$ and $\Gamma_0 = \lim_{r\to\infty}\Gamma$; and from (1) and (3), provided that $r\overline{v_r' v_z'} \to 0$ as $r \to \infty$,

$$2\pi \int_0^\infty \{v_z(v_z - 1) - \tfrac{1}{2}v_\theta^2 + \overline{v_z'^2} - \tfrac{1}{2}(\overline{v_r'^2} + \overline{v_\theta'^2})\}\, r\,\mathrm{d}r = F. \tag{6}$$

The vortex is thus characterized by the sum of the axial mean momentum flux and the pressure thrust, termed the flow force $F\rho c^2 U^2$, and the circulation $\Gamma_0 cU$; but note that, while $F$ and $\Gamma_0$ are conserved, the fluxes of mean axial momentum and mean angular momentum are not (Morton 1969). For the case where the vortex is still in the process of rolling up, (5) and (6) take on a slightly different form, since the upper limit of integration must be interpreted as the radius to which successive turns of the vortex layer have merged, and this radius, $\Gamma_0$ and, indeed, $F$ are functions of $z$. However, provided that the asymptotic roll-up process is well advanced, the variation in $F$ is likely to be small, and possibly less than any error involved in measuring it.

Now as the tangential velocity decays, an axial pressure gradient develops, and with it an axial component of flow (Batchelor 1964). Morton shows that the axial pressure gradient is important if $F \sim \Gamma_0^2$ and negligible if $F > \Gamma_0^2 z\,Re$; so to scale its importance we employ Long's (1961) parameter $F/\Gamma_0^2$. Then the first condition suggests, in its limit, that $F/\Gamma_0^2 = 1$, and the latter that $F/\Gamma_0^2 > z\,Re$. In the present study we restrict attention to trailing vortices for which $F/\Gamma_0^2 = O(1)$, as it is these that are most likely to occur in free flight (see McCormick, Tangler & Sherrieb 1968; Verstynen & Dunham 1973).

## 3. Experimental procedure

### 3.1. *General*

The experiments were performed in an open-return circular blower tunnel (described in detail by Vogel 1968) located in the air-conditioned Low-Speed Aerodynamics Laboratory at McGill University. Dripac high-efficiency air filters at the tunnel entrance removed dust particles larger than 1 μm, and provided a resistance high enough to ensure that the flow in the 0.762 m diameter, 6.4 m long working section was little affected by conditions in the laboratory near the tunnel inlet. The walls of the working section were of porous-metal sheet and the distribution of porosity was arranged (by judicious blanking of the perforations with paper tape) to give an almost zero streamwise pressure gradient (within ±3 % of dynamic pressure over 5 m) along the tunnel axis with the vortex absent. Free-stream turbulence† $v_z^*$ was about 0.5 %.

The vortex generator was mounted horizontally across the throat of the wind-tunnel contraction (see figure 1) and consisted of two identical wings‡ (see figure 2) set at equal (as viewed from the axis of symmetry) angles of incidence. The wings were designed (by Poppleton) to maintain constant circulation except at the tips, where, over a radius of 5 cm, a sinusoidal-like transition connected the positive circulation of each to zero at the axis, thereby generating a region of high vorticity and a vortex sheet that rolled up into a double-branched spiral (see Pullin & Phillips 1981). To foster the development of turbulent boundary layers on the wings, and thereby suppress separation, a trip wire was placed ahead of each. The wings were linked by a nacelle enclosing a 9.5 mm internal-diameter pipe that supplied the jet (via a compressed air source) and supported the bluff body used to enhance the wake (see figure 2).

† N.B. $v_i^* \equiv (\overline{v_i'^2})^{\frac{1}{2}}$ $(i = r, \theta, z)$.

‡ With chord $c = 5.08$ cm.

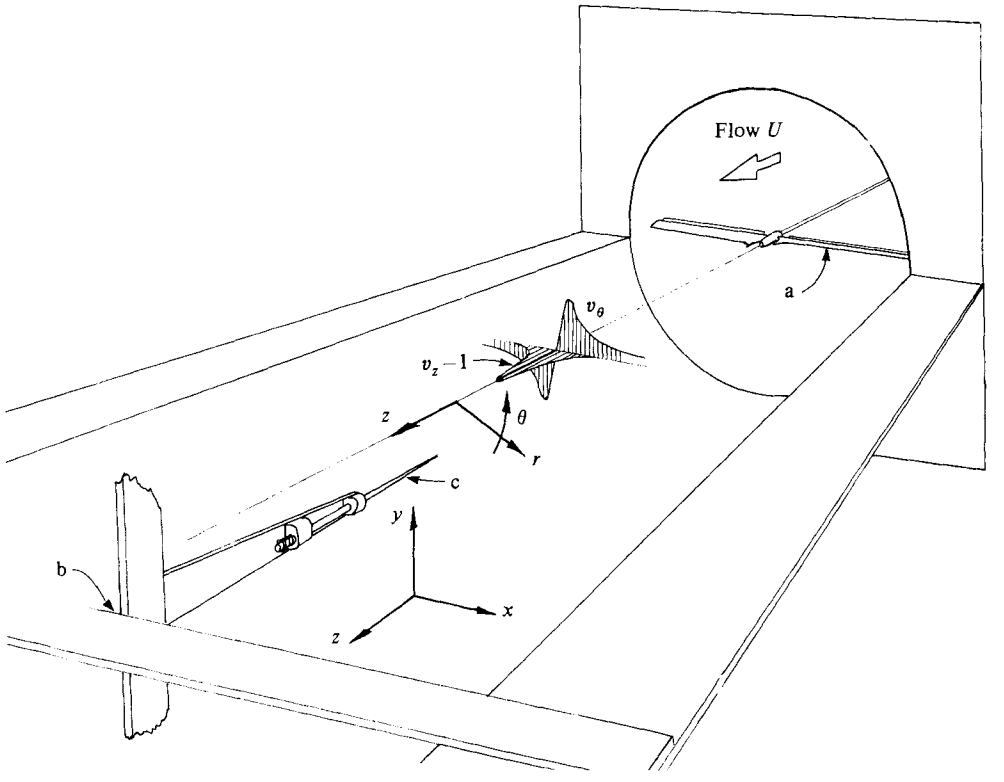


FIGURE 1. View of circular blower tunnel with upper portion removed to expose: a, the wings (detailed in figure 2); b, the traverse gear; and, c, the probe holder.

The traverse gear moved on a horizontal streamlined bar set into the working section, and allowed horizontal and vertical movement over a large cross-sectional area. The probe holder, a long, narrow, slowly tapering device (see figure 1), positioned the hot wire some 570 mm upstream of the traverse gear and was designed to minimize interference; in effect, to increase the dynamic pressure at the probe by less than 1%. The probe could be rotated azimuthally; and this was done in increments of 45° by a servo motor.

Accurate spatial location (to less than 0.1 mm) and initial orientation in azimuthal angle (to less than $\pm 1°$) of the probe was straightforward, but precise alignment in the critically important pitch and yaw was not. This was achieved after careful geometrical orientation followed by fine adjustments based on the mean output of an inclined hot wire at a variety of azimuthal angles in streaming flow; when correctly aligned the output of the hot wire is independent of azimuthal angle. In practice, alignment was altered to minimize the errors at four cross-stream locations. The final alignment was estimated to be accurate to within $\pm\frac{1}{4}°$ in pitch and yaw.

Measurements were made at specified points, and a group of measurements in line either horizontally or vertically constituted a traverse; traverses were generally performed at three downstream stations: $z = 45$, 78 and 109 at constant $U$.

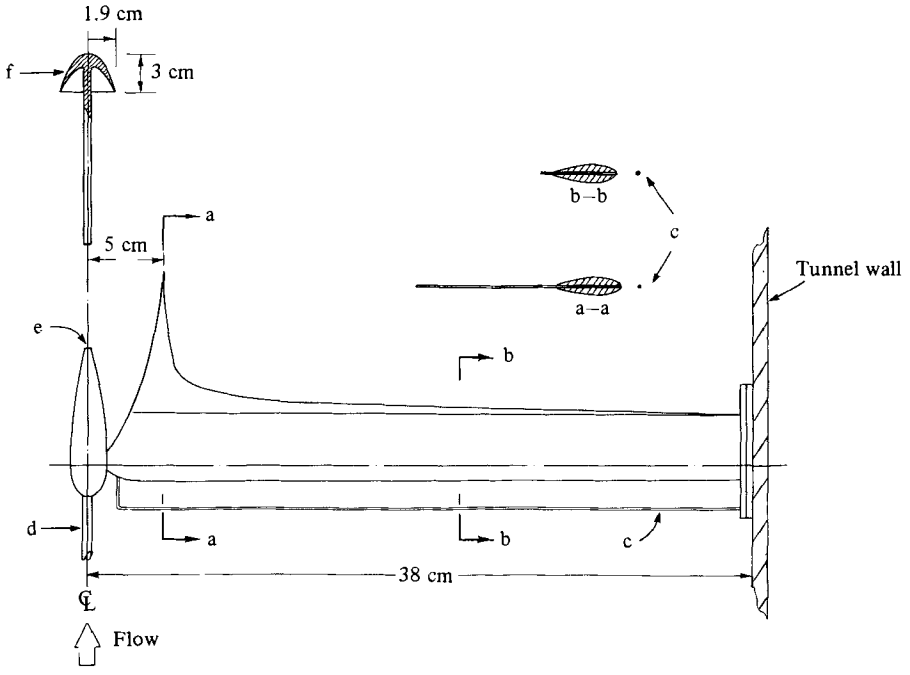


FIGURE 2. The vortex generator, showing: c, the trip wire; d, the 0.952 cm jet pipe; e, the jet outlet; and, f, the bluff body used in case E to enhance the wake (see §4.1) and which plugs into the jet outlet.

### 3.2. *Data acquisition*

DISA 55A22 (normal) and 55A25 (inclined) hot-wire probes connected with 5 μm tungsten wire were used throughout, and each was connected to a DISA model 55D01 constant-temperature anemometer unit coupled to a 55D10 linearizer. After filtering frequencies above 20 kHz (with a DISA 55D25 filter), the linearized signal passed to a DISA type 55D35 r.m.s. meter. To ensure that the anemometers, linearizers, etc. remained in a state of thermal equilibrium, they were neither switched off nor moved throughout the series of experiments.

Output from the linearizer–anemometer combination was calibrated against a range of velocities, as measured by Pitot and Pitot–static tubes. The Pitot tubes and the hot-wire probe were positioned 2.54 cm apart in the wind tunnel, at a standard location well away from the wake of the vortex generator, which was set to zero incidence. The calibration constants pertaining to the hot wire were found to be repeatable and stable, and thus required only periodic checking. But at various times during a traverse the linearizer–anemometer output was checked against a standard velocity, that of streaming flow without a vortex, at the abovementioned calibration location. Dust filtering and almost-constant air temperature contributed significantly toward the stability of calibration. Inclined wires were calibrated in yaw and pitch in Smith's (1973) calibration drum; and the pitch angle was measured using a 50 × Nikkor profile projector.

The Pitot and Pitot–static tubes were also used to calibrate a Statham pressure transducer; this monitored the tunnel speed by measuring the difference in static pressure between the throat of the tunnel contraction and the settling chamber.

### 3.3. *Data reduction*

The outputs from the linearizer, r.m.s. meter and pressure transducer were linked, via high-quality triple-shielded cable, to a VIDAR integrating digital voltmeter interfaced to a GEPAC 4020 minicomputer. The VIDAR integrated readings over 16.6 ms and then summed the result over 10 s. The summed readings were then stored by the computer, which simultaneously controlled the whole procedure. On completion of each experiment a further program retrieved the stored information and transformed it into the desired velocity and Reynolds-stress information.

The equations required for this reduction follow from the analysis of Champagne & Sleicher (1967) (for the response of an inclined hot wire to three-dimensional flow), but taken to higher order and with corrections for blockage and yaw, in addition to the previously included pitch (see Phillips 1984). Such modifications were felt desirable in view of the scatter and low values of the cross-coupled terms reported by Poppleton. Corrections for blockage and yaw were found to be minor, but the higher-order corrections were not: indeed, the correction for the most offending shear stress $\overline{v_x' v_y'}$ includes two other shear stresses, two intensities and two velocity components, and could not be ignored.

As input to these equations, we require, at each point, mean and fluctuating readings from an inclined wire at six azimuthal angles, $\phi$ (viz $\phi = 0°$, 45°, 90°, 135°, 180° and 270° measured from the horizontal), and similar readings from a normal wire at one azimuthal angle. The readings were obtained by making an entire traverse with a normal wire, followed by an identical traverse with an inclined wire. The results are referred to a rectangular Cartesian coordinate system ($cx$, $cy$, $cz$) (see figure 1) with velocity components ($Uv_x$, $Uv_y$, $Uv_z$); $y$ is vertical, $z$ is streamwise.

The terms $\overline{v_x'^2}$ and $\overline{v_y'^2}$ derive from the sum of two mean-squared readings (from an inclined wire) 180° apart, while $\overline{v_z'^2}$ derives from one mean-squared reading at $\phi = 90°$ with a normal wire. The cross-correlations all derive from differences between two mean-squared readings: for $\overline{v_x' v_z'}$ and $\overline{v_y' v_z'}$ the readings are 180° apart, while for $\overline{v_x' v_y'}$ they are 90° apart.

At each point nine pieces of information were derived from fourteen pieces of raw data; the redundant data were used during the initial stages as a guide to eliminating computational and experimental errors. In the final data-gathering process the most direct way of determining each parameter was chosen although, as a check, $v_z$ was always evaluated by independent methods.

### 3.4. *The vortex axis*

We should like to view the measurements in terms of the cylindrical coordinates of §2, and the necessary transformation is

$$\begin{pmatrix} v_r \\ v_\theta \end{pmatrix} = ([x-x_0)^2+(y-y_0)^2]^{-\frac{1}{2}} \begin{pmatrix} x-x_0 & y-y_0 \\ y_0-y & x-x_0 \end{pmatrix} \begin{pmatrix} v_x \\ v_y \end{pmatrix}. \tag{7}$$

But to utilize (7) we require the coordinates (relative to the traversing system) of the vortex axis, $(x_0, y_0)$ say. And although $(x_0, y_0)$ may be deduced *a posteriori* from measurements of $v_x$ and $v_y$, and then used in (7), it is better to locate the vortex axis from preliminary measurements, and traverse through it; and we did so.

The axis was found in two ways: first, by using a 1.6 mm diameter Pitot tube to locate the point of greatest total-head deficit; secondly, by taking hot-wire traverses of $v_x$ and $v_y$ near the axis and making use of (7). The respective methods yielded points less than 1.5 mm apart.

Mason & Marchman (1972) report that 'moving the probe in the[ir] vortex caused the vortex to move'. No such motion is apparent here. If there were, the Pitot tube and hot-wire probe, which were mounted 2.54 cm apart, would locate the vortex centre at markedly different points in space.

Finding the vortex axis was considerably simplified when jets or wakes were imposed on the vortex, since exploratory measurements indicated that their axes were coincident and that its position was very nearly constant from flow to flow. To find the axis of the flow, therefore, it was sufficient to determine the centreline of the jet or wake by mapping $v_z$ with a normal hot wire. But, although great care was taken to locate the axis, it is presumptuous to claim that it was always traversed; it is fair to say, however, that, for a traverse along $y$, $y-y_0 \ll r_1$ at $x-x_0 = 0$, where $cr_1$ is the radius at which the tangential mean velocity takes its peak value $Uv_1$. Moreover, with an error of this magnitude, we see from (7) that only negligible corrections are required to all transformations except $\overline{v_r' v_\theta'}$, so that it is reasonable simply to assume that the vortex axis was traversed. For $\overline{v_r' v_\theta'}$,

$$\overline{v_r' v_\theta'} = \{\overline{v_x' v_y'}[(x-x_0)^2-(y-y_0)^2]-(\overline{v_x'^2}-\overline{v_y'^2})(x-x_0)(y-y_0)\}[(x-x_0)^2+(y-y_0)^2]^{-1}, \tag{8}$$

so for $y-y_0 \neq 0$ we have that $\overline{v_r' v_\theta'} = -\overline{v_x' v_y'}$ at $r = y-y_0$ and that $\overline{v_r' v_\theta'}$ is undefined for $0 < r < y-y_0$; while for $r \to \infty$, $\overline{v_r' v_\theta'} \sim \overline{v_x' v_y'}$. Thus close to the origin our $\overline{v_r' v_\theta'}$ data must be viewed with caution.

### 3.5. *Test flows*

The experimental and reduction procedures were tested by taking measurements in two well-documented flows; fully developed turbulent flow in a circular pipe and the turbulent round jet discharging into still air.

In the pipe flow the measured shear-stress profile corresponds almost exactly to that calculated from the pressure drop, and the turbulence intensities are in accord with those measured by Guitton (1968) and Irwin (1972) in the same pipe.

The physical configuration for the round jet was made as close as possible to that of Wygnanski & Fiedler (1969). Near the flow axis (where no high-turbulence-level corrections were necessary) our measured Reynolds-stress field was similar in form to theirs, but of lower apparent level. For example $v_z^*$ on the axis 75–100 outlet diameters downstream was 0.24 compared with their 0.28. This was due to the limited response of our r.m.s. meter below 0.5 Hz. In the present work, however, this is not expected to be important, since the lowest frequencies of interest are an order of magnitude higher than those in the round jet.

## 4. Experimental results

### 4.1. *Cases studied*

Experimental flows consisted of trailing vortices coaxial with either an imposed jet or wake. The vortex generator was inclined at 9° to the streaming flow, the velocity of which was 21.4 m/s; in all cases $\Gamma_0 \approx 0.74$. Traverses were made in the region $-4 < x-x_0 < 4$ for all cases at $z = 45$, 78 and 109, yielding, for $z/\Gamma_0$, the respective values 61, 105 and 147. The following cases were studied:

Case A: a strong jet, with a stagnation pressure of $1.2 \times 10^2$ kN/m$^2$, in which the peak velocity increment at the first station ($z = 45$) was 26 % of the free-stream velocity; $F/\Gamma_0^2 \approx 5$.

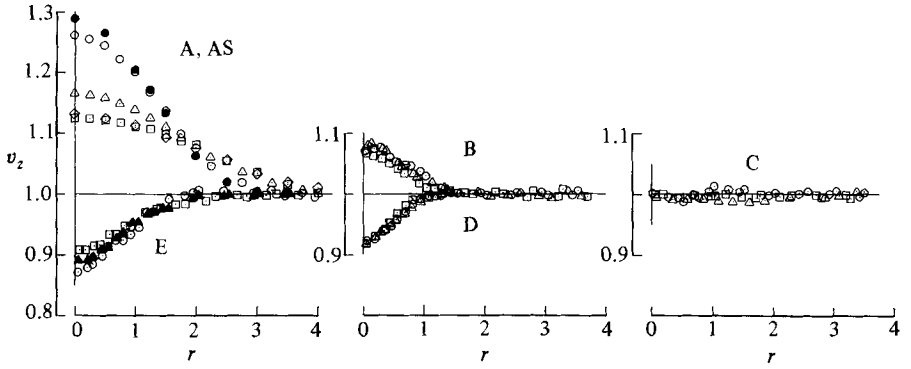


FIGURE 3. Axial-velocity profiles: symbols for cases A, B, C, D, E: ⊙, $z = 45$; △, $z = 78$; ⊡, $z = 109$. For case AS: ●, $z = 45$; ◇, $z = 109$.

| | $z = 45$ | | $z = 78$ | | $z = 109$ | |
|---|---|---|---|---|---|---|
| Case | $A$ | $b$ | $A$ | $b$ | $A$ | $b$ |
| A | 0.26 | −0.33 | 0.165 | −0.20 | 0.125 | −0.15 |
| AS | 0.29 | −0.38 | — | — | 0.135 | −0.164 |
| B | 0.075 | −1.23 | — | — | — | — |
| D | −0.08 | −2.29 | — | — | — | — |
| E | −0.13 | −0.89 | −0.115 | −0.78 | −0.09 | −0.67 |

TABLE 1

Case AS: the same jet as in case A but with no vortex; $F \approx 2.75$.

Case B: a significantly weaker jet (with a stagnation pressure of $0.22 \times 10^2$ kN/m$^2$) having similar half-width as the wake in case D. Here the peak velocity increment was 7.5% of $U$ at $z = 45$ and $F/\Gamma_0^2 \approx 0.22$.

Case C: a jet whose momentum flux was just sufficient to eliminate the momentum deficit of the unmodified wake (case D). Thus, after a certain period it produced a field of approximately uniform axial mean velocity, thereby approximating a line vortex; $F/\Gamma_0^2 \approx -0.12$.

Case D: the wake resulting from the vortex generator and nacelle assembly, for which the peak velocity decrement was 8% of $U$; $F/\Gamma_0^2 \approx -0.32$.

Case E: a wake enhanced by a 0.38 mm diameter cup-shaped bluff body, lips upstream, fixed to the central nacelle (see figure 2). It was intended that this wake should have an axial-momentum decrement and half-width similar in magnitude to those of case A, but in practice this proved unattainable. The abovementioned cup gave a wake where $|F/\Gamma_0^2|$ was several times greater than in case D, though smaller than in case A. Here the peak velocity decrement was 13% of $U$ at $z = 45$ and $F/\Gamma_0^2 \approx -0.9$.

### 4.2. *Axial mean-velocity profiles*

The axial mean-velocity profiles are given in figure 3. With the exception of case C, in which $v_z \approx 1$, all are roughly Gaussian distributions, and for computational purposes are well described by $v_z = 1 + A\,e^{br^2}$. Appropriate $A$- and $b$-values are given in table 1.

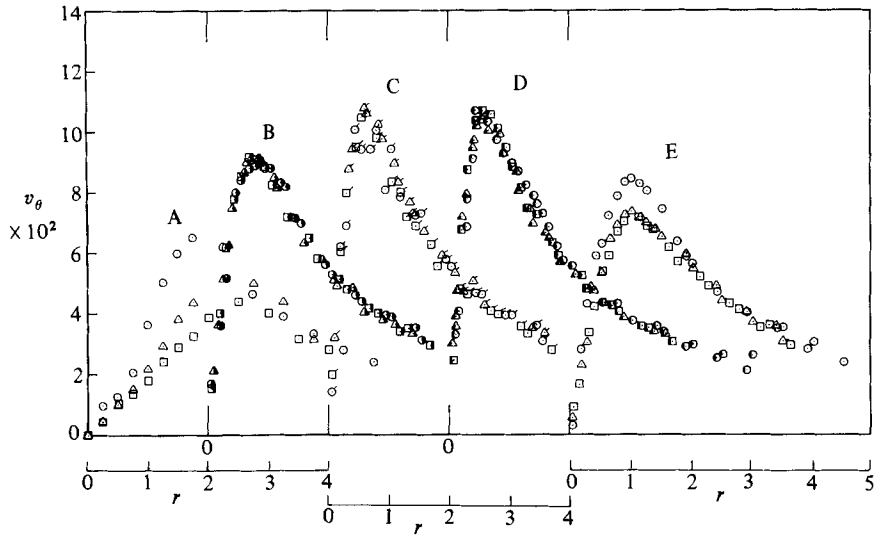


FIGURE 4. Tangential velocity profiles for cases A, B, C, D, E respectively: ⊙, ◑, ⊙, ◐, ⊙, $z = 45$; △, ▲, △, ▲, △, $z = 78$; ⊡, ◨, ⊡, ◧, ⊡, $z = 109$.

Case AS undergoes the greatest decay and radial spread, but quantified as the rate of change of the jet half-width $r_{\frac{1}{2}}$ with $z$, we find $r_{\frac{1}{2}}/(z-z_0) \approx 0.014$ (where $z_0$ is the virtual origin of the jet), a value much lower than that for a round jet into stagnant surroundings, which is typically 0.09 (Ribeiro & Whitelaw 1980). Growth of the same jet with a vortex (case A) is even slower ($\approx 0.01$), but such behaviour should not be interpreted as typical because, as is clear from (6), the development of the axial and tangential velocity fields are coupled.

There is a slow but perceptible downstream change in $v_z$ for cases B and E, while cases C and D remain virtually constant.

### 4.3. *Tangential mean-velocity field*

The tangential mean-velocity profiles are given in figure 4. All are characterized by a central core of close to solid-body rotation surrounded by an annulus of high strain rate. Those flows with the greatest $|F/\Gamma_0^2|$, whether caused by imposing a jet (case A) or a wake (case E) on the vortex experience the greatest diminution of the tangential velocity field, and thus $v_1$; while cases B, C and D, for which $|F/\Gamma_0^2| \ll 1$, remain almost unchanged. Poppleton (1971*a*, *b*) and Mason & Marchman (1972) report similar behaviour. Cases C and D have roughly equal, and the highest, values of $v_1$.

Comparison of horizontal ($-4 < x-x_0 < 4$) and vertical ($-4 < y-y_0 < 4$) traverses (for both cases A and D) at $z = 45$) indicated that the mean-velocity field was continuous and close to axisymmetric, and showed that the innermost part of the double-branched spiral, formed by the rolling-up vortex layers, had merged (see Phillips 1981).

On physical grounds we should expect the point of highest axial vorticity to be at the vortex axis, and this is so for all cases except A. Here, an inner core of close to solid-body rotation is surrounded by an annulus of greater angular velocity, which then merges into the highly sheared region where $v_1$ occurs. At successive downstream stations, the region of solid-body rotation expands into the neighbouring annulus without itself being speeded up, and by $z = 109$ occupies the entire rotational region

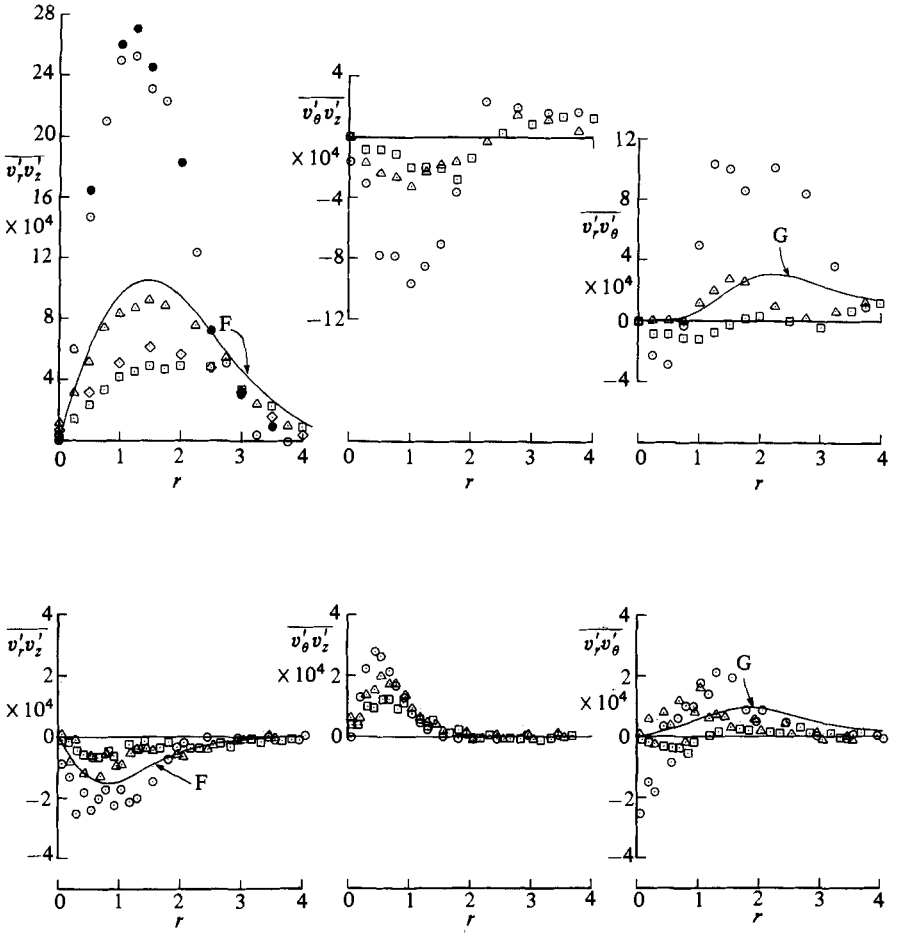


FIGURE 5. Reynolds shear stress profiles for cases A and E. Symbols as in figure 3. F, profile calculated by difference from (3) at $z = 78$; G, as before, using (2).

to $r_1$. Moreover, at the first two stations the value of $\Gamma$ is, for $r > r_1$, in excess of the $\Gamma_0$ value exhibited by the other flows.

The necessity for overcirculation (i.e. $\Gamma > \Gamma_0$) in turbulent line vortices is clear from Saffman's Theorem (see Govindaraju & Saffman 1971), but the theorem requires large $z$; a condition not met here. This does not preclude overcirculation, however, because in a turbulent trailing vortex if $z \ll Re$ then from (5)

$$\int_0^\infty (\Gamma - \Gamma_0) v_z r \, dr \approx \text{const}, \tag{9}$$

indicating that $\Gamma$ and $v_z$ are strongly coupled and that $\Gamma > \Gamma_0$ is admissible over some $r$; although inducing overcirculation in this way may be restricted to contrived situations such as case A, where the vortex is flooded by a rapidly decaying jet.

### 4.4. *Reynolds stresses*

The turbulence intensities and Reynolds shear stresses are given in figures 5–8; the first two exhibit data for the extreme cases A and E, the latter two the intermediate cases B–D.

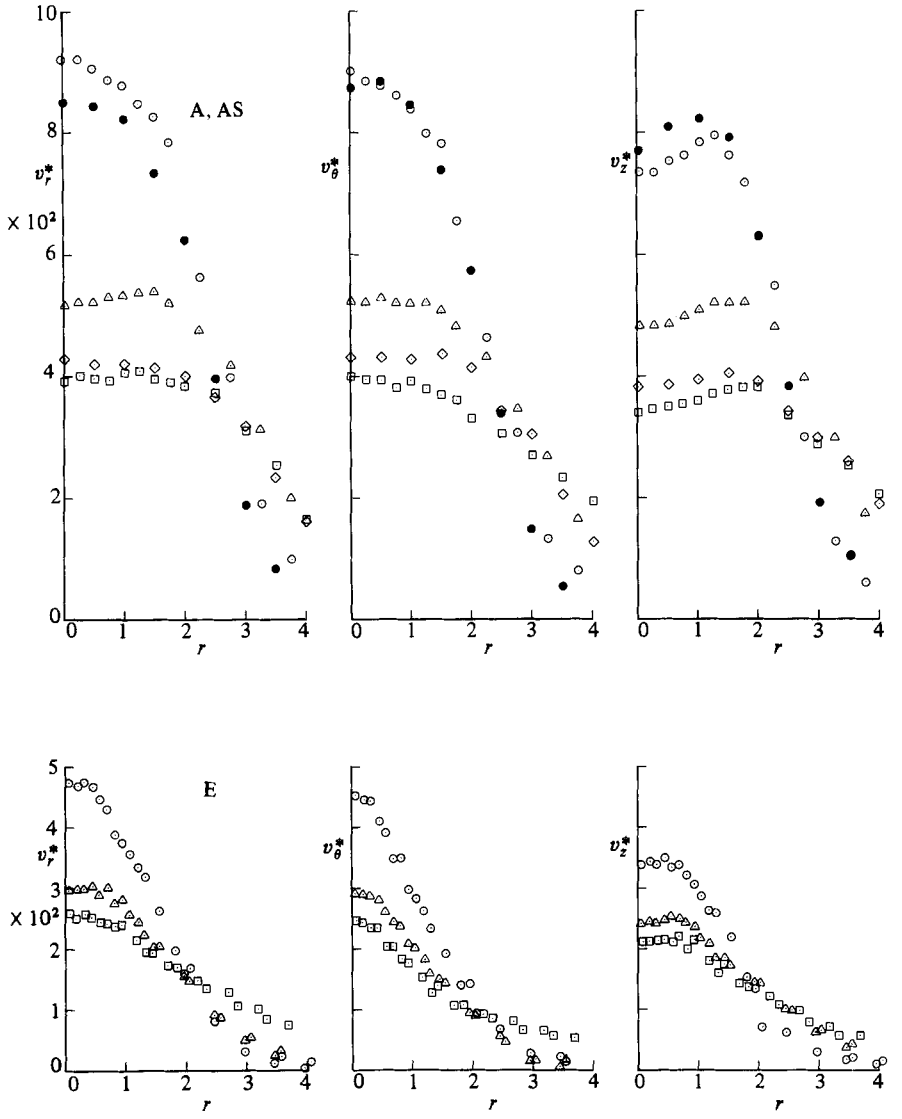


FIGURE 6. Turbulence intensities for cases A, AS and E. Symbols as in figure 3.

Looking first at figure 5, we see that the $\overline{v_r' v_z'}$ profiles are typical of those for axisymmetric jets and wakes, being positive for the former and negative for the latter. Moreover, they agree well with the profiles calculated from (3), which are based upon the measured velocity field (see §4.5). It would appear that $\overline{v_r' v_z'}$ is slightly higher for case AS than for case A; this could be attributed to the axial pressure gradient present in case A and not in case AS. Note also that the stress levels of case E are almost an order of magnitude lower than in case A, in accord with the much lower decay rate of case E's axial velocity field.

The shear stress $\rho \overline{v_\theta' v_z'}$ is of opposite sign to the $\overline{v_r' v_z'}$ component (although for case A it changes sign for some $r > r_1$). Such behaviour contrasts markedly with that for a swirling jet, in which $\overline{v_\theta' v_z'}$ and $\overline{v_r' v_z'}$ are of the same sign (see Pratte & Keffer 1972; Morse 1979).

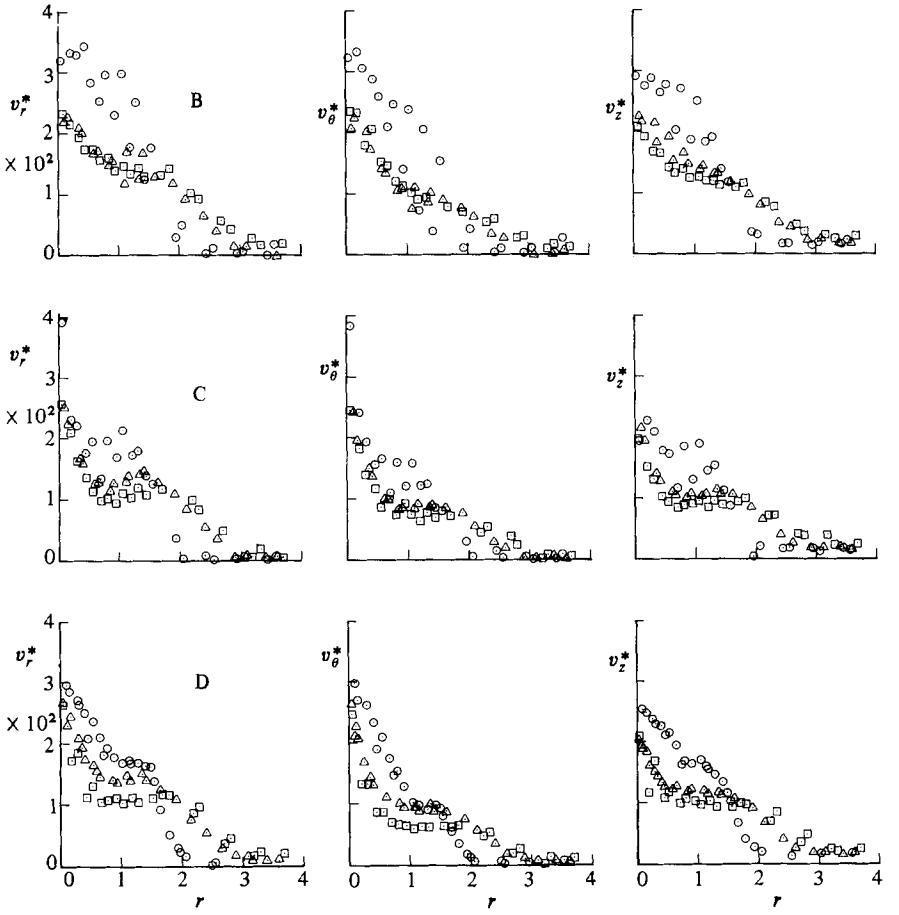


FIGURE 7. Turbulence intensities for cases B, C and D. Symbols as in figure 3.

The profiles for $\overline{v_r' v_\theta'}$ at $z = 78$, calculated from (2), are in fair agreement with the data, which is noteworthy in view of the difficulties and corrections associated with measuring them. This stress is seen to decrease rapidly with $z$, particularly in case A, and, for most cases, to change sign at some $r < r_1$. Singh's (1974) data for $\overline{v_r' v_\theta'}$ are positive for all $r$.

Turning now to the turbulence intensities (figure 6), we note that axisymmetry requires $v_r^* = v_\theta^*$ at $r = 0$ and that the measurements closely conform. Not surprisingly, the intensity levels are highest, and the decay most rapid, for cases A and AS.

Now for a round jet into stagnant surroundings $v_z^* > v_\theta^* \geqslant v_r^*$ over the radius of the jet (Wygnanski & Fiedler 1969); however, for our jet into streaming flow (case AS) we find $v_\theta^* \geqslant v_r^* > v_z^*$, and, on adding the vortex (case A), $v_r^* \geqslant v_\theta^* > v_z^*$ for some $r < r_1$ and $v_r^* > v_z^* > v_\theta^*$ for $r > r_1$. Such behaviour is also true for cases B–E. The situation where $v_r^*$ is greater than both $v_\theta^*$ and $v_z^*$ is typical of flows in which turbulence production is significantly less than diffusion, such as in the central region of an axisymmetric wake.

The turbulence intensities for cases B–D are given in figure 7. Again the axisymmetry constraint at $r = 0$ is closely met; however, away from the origin the B and

C readings at $z = 45$ are not axisymmetric, although they become so by $z = 78$. Such behaviour is not uncommon in free turbulent shear flows, because Reynolds stresses take time to be generated and time to decay, so that local axisymmetry of the mean-velocity field need not imply local axisymmetry of the stresses (Townsend 1976).

The turbulence levels for cases B–D do not vary greatly from case to case, nor with $z$. All peak in the region $r < r_1$, possibly in consequence of the turbulent boundary layer on the nacelle surrounding the jet pipe (see figure 2). According to Rayleigh's criterion the flow in this virtually solid-body region is highly stable, so that any turbulence there should rapidly decay. It doesn't! This result is contrary to that of Barker & Crow (1977), who observed laminar annuli at the centres of their nominally two-dimensional vortex pairs. The reason for the discrepancy may well be due to the details of each flow: Barker & Crow took considerable care to minimize three-dimensional effects, so that Rayleigh's criterion, which is strictly two-dimensional, should apply. Our flow is three-dimensional and columnar, where destabilization can occur in the presence of axial flow owing to azimuthal disturbances (Leibovich & Stewartson 1983); and we have both azimuthal disturbances and axial flow, even in case C.

Measurement of Reynolds shear stress involves subtraction of two hot-wire signals, so that the likelihood of error increases when the signals, and their differences, are small. However, in spite of these terms being of the order of $10^{-5}$ (see figure 8) some sensible profiles were obtained, particularly for case B, where each shear stress (with the exception of $\overline{\rho v_r' v_\theta'}$ at $z = 45$, which is not symmetrical) apes its counterpart in case A. For cases C and D only $\overline{v_\theta' v_z'}$ exhibits simple distinct profiles; $\overline{v_r' v_z'}$ and $\overline{v_r' v_\theta'}$ appear erratic, although some downstream similarities are present, particularly for $\overline{v_r' v_z'}$. Note that the curves depicted in figure 8 were sketched by eye; they have no theoretical basis.

### 4.5. *Momentum balance*

We have enough information to evaluate each term in the mean momentum equations (1)–(3) at $z = 78$, and do so for the two extreme cases A and E (see figures 9 and 10). By difference we find, from (1), $\partial p/\partial r$; from (2), $\partial(r^2\overline{v_r' v_\theta'})/r^2\,\partial r$; and, from (3), $\partial(r\overline{v_r' v_z'})/r\,\partial r$. The ensuing $\overline{v_r' v_\theta'}$ and $\overline{v_r' v_z'}$ profiles are plotted in figure 5.

Now in the analysis of a trailing vortex one would normally apply an assumption of the boundary-layer type, i.e. $\partial/\partial z \ll \partial/\partial r$, which requires $v_r \ll v_z$, a result supported by the present work; compare figures 3 and 11. Equation (1), which is used to evaluate $\partial p/\partial z$ in (3), then becomes

$$\frac{\partial p}{\partial r} = \frac{v_\theta^2}{r} + \frac{\overline{v_\theta'^2} - \overline{v_r'^2}}{r} - \frac{\partial \overline{v_r'^2}}{\partial r}.$$

The balance $\partial p/\partial r = v_\theta^2/r$ would next be assumed on the basis that $\overline{v_\theta'^2} \approx \overline{v_r'^2}$ (which is reasonable, see figure 6) and that $\partial\overline{v_r'^2}/\partial r$ may be neglected. But $\partial\overline{v_r'^2}/\partial r$ may not be neglected (figure 9), since the high turbulence intensities introduced by the jet fall rapidly with increasing $r$ and lead to a situation where $v_\theta^2/r$ and $\partial\overline{v_r'^2}/\partial r$ are numerically almost equal over some $r$, thereby affecting $\partial p/\partial r$.

Turning now to the $\theta$-wise momentum equation (2), we find that the term of most interest is $\partial(r^2 v_r v_\theta)/r^2\,\partial r$. Observe that although $v_r$ made only negligible contributions to (1), it is clear from figures 9 and 10 that terms containing it in (2) *cannot be ignored*; doing so would affect the vortex decay rate. From an analyst's point of view this

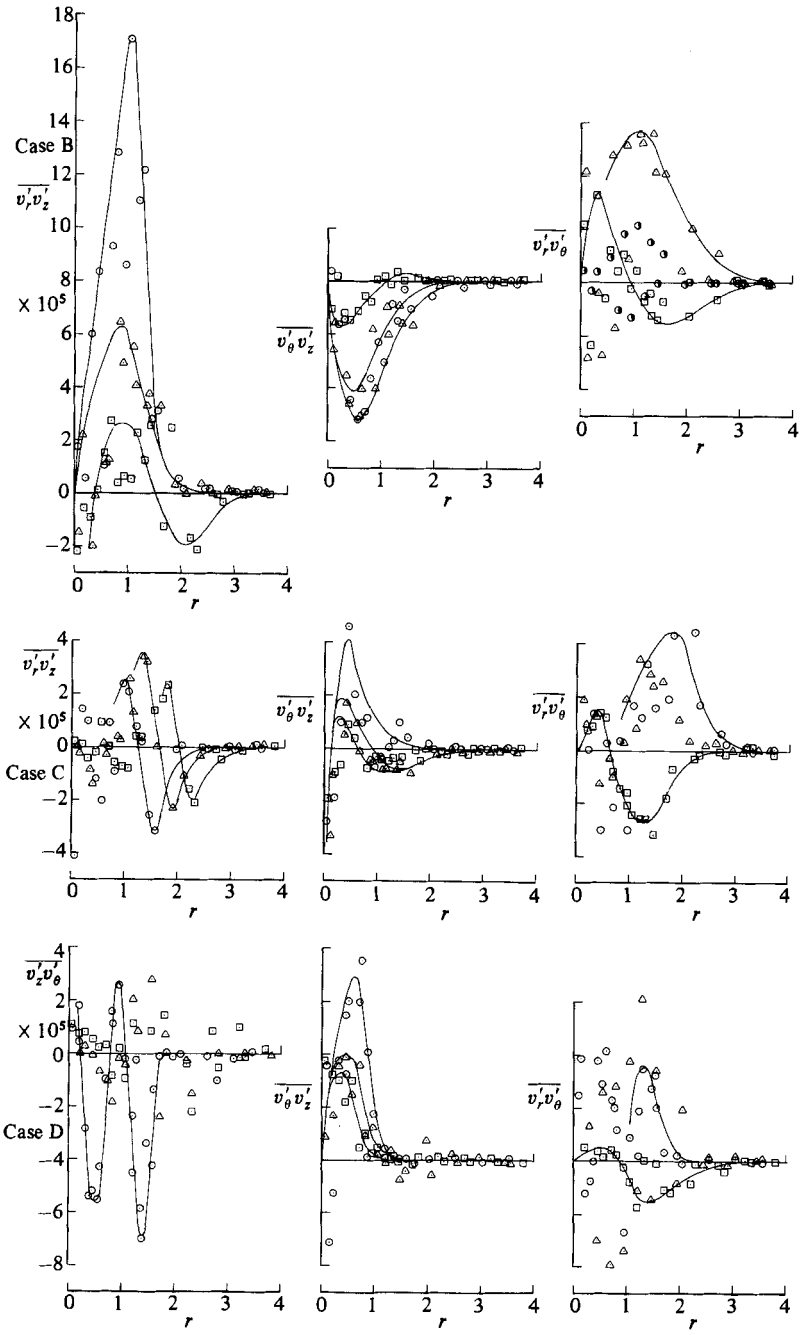


FIGURE 8. Reynolds shear stresses for cases B, C and D. Symbols as in figure 3. The ordinate for the extra symbol ◑ at $z = 45$ is multiplied by ten.

means that the inertia terms in (2) and (3) may not be linearized – unless $|F/\Gamma_0^2| \ll 1$, as in cases B–D (see §5).

The importance of $v_r$ is further exemplified by the balance of terms in the axial-momentum equation (3). Here we find (for both cases A and E), that $\partial(rv_r v_z)/r\,\partial r \approx \partial(r\overline{v_r'v_z'})/r\,\partial r$ and that both contribute significantly to (3), while the

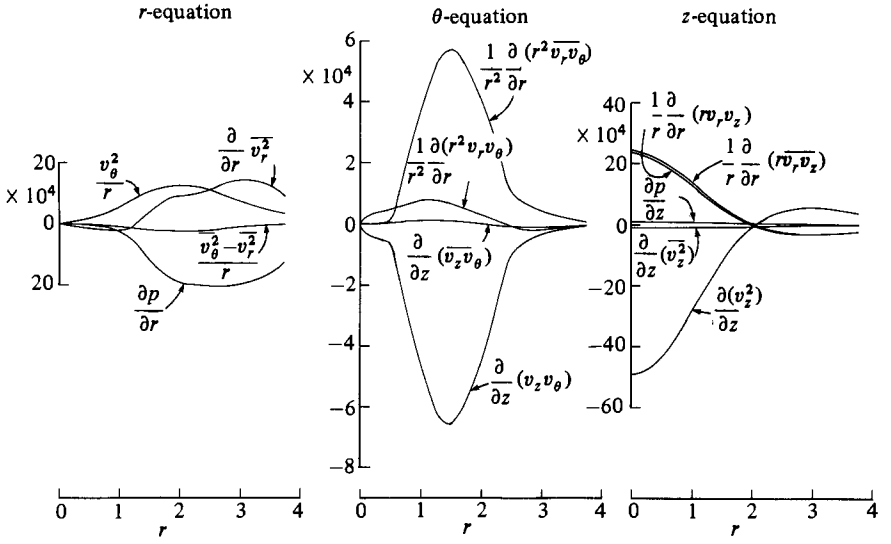


FIGURE 9. Momentum balance for case A.

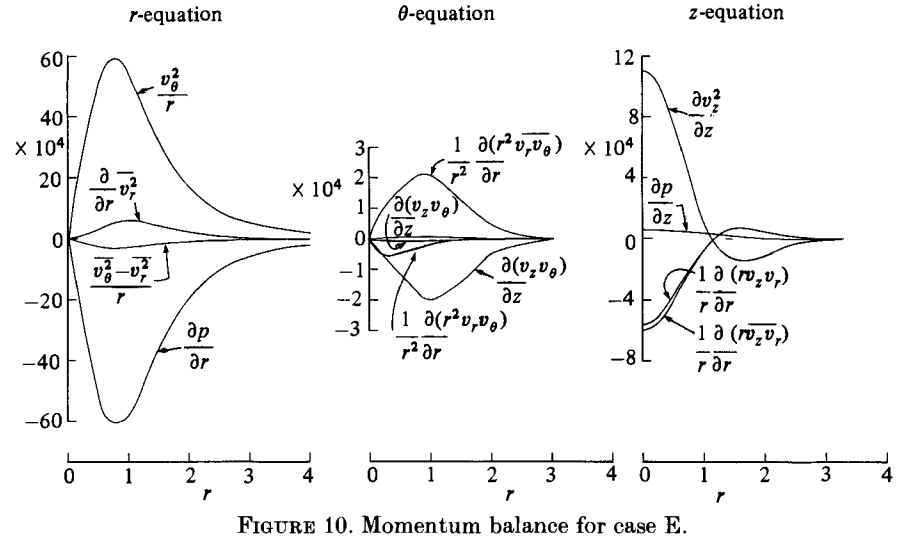


FIGURE 10. Momentum balance for case E.

axial pressure gradient, induced by the decaying circumferential velocity, is relatively minor. But because $\partial p/\partial z$ is numerically much smaller than other terms in (3) does not mean it can be ignored, for, as Batchelor (1964) notes, it has a cumulative effect on the axial-velocity field over large $z$.

## 5. Discussion

It is well known that blowing a jet along the axis of a trailing vortex increases the radial dispersal of vorticity, presumably by increasing the level of turbulence. So if the turbulence level is increased by other means, creating a wake for example, we

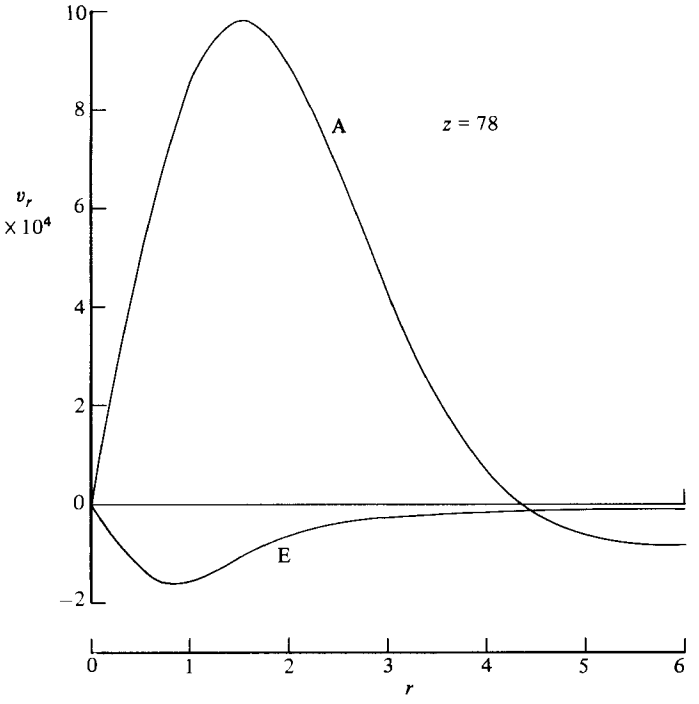


FIGURE 11. Radial-velocity profiles at $z = 78$ for cases A and E as calculated from (4).

might expect similar behaviour. The experiments bear this out, but they also indicate that imposing a wake is less effective in dissipating vorticity than imposing a jet.

We see why from trajectories of sectional mean streamlines† in the plane normal to the vortex axis. Observe that for case E (figure 12) the trajectories spiral inward to a focus at the origin, indicating that the vortex is being longitudinally stretched (Perry, Lim & Chong 1980). The vorticity of each of the myriad vortex lines that compose the trailing vortex is thus increased, so that the effect of their radial dispersal by turbulence is then to some extent reduced.

Imposing a jet, however, subjects the vortex to longitudinal compression, which diminishes the level of vorticity in each of the composite vortex lines and, coupled with their radial dispersal by turbulence, acts to enhance vortex decay. Thus the tangential velocity in case B (which is compressed and in which the turbulent intensities and velocity increments are roughly equal to the magnitude of case D's) is seen by $z = 109$ to have decayed more than case D, whose state of decay (due to stretching) is not dissimilar to that of case C, which is unstretched.

Sectional mean streamlines are concentric circles for an unstretched vortex (see case C, figure 12), while for longitudinal compression they spiral out from the origin. The spiral is unbounded only if the vortex grows at the rate $(\nu t)^{\frac{1}{2}}$, however (see (5)), as faster growth necessitates stretching over some $r > r_1$. Stretching increases the angular momentum there at the insistence of (5), following the depletion of angular

† Streamlines based on the velocity field in the plane of the section. Those for cases A and E at $z = 78$ were obtained by Runge–Kutta integration using relevant velocities from figures 4 and 11, but for schematic reasons the azimuthal ordinate in figure 12 has been reduced by approximately 6 for case A and 60 for case E.

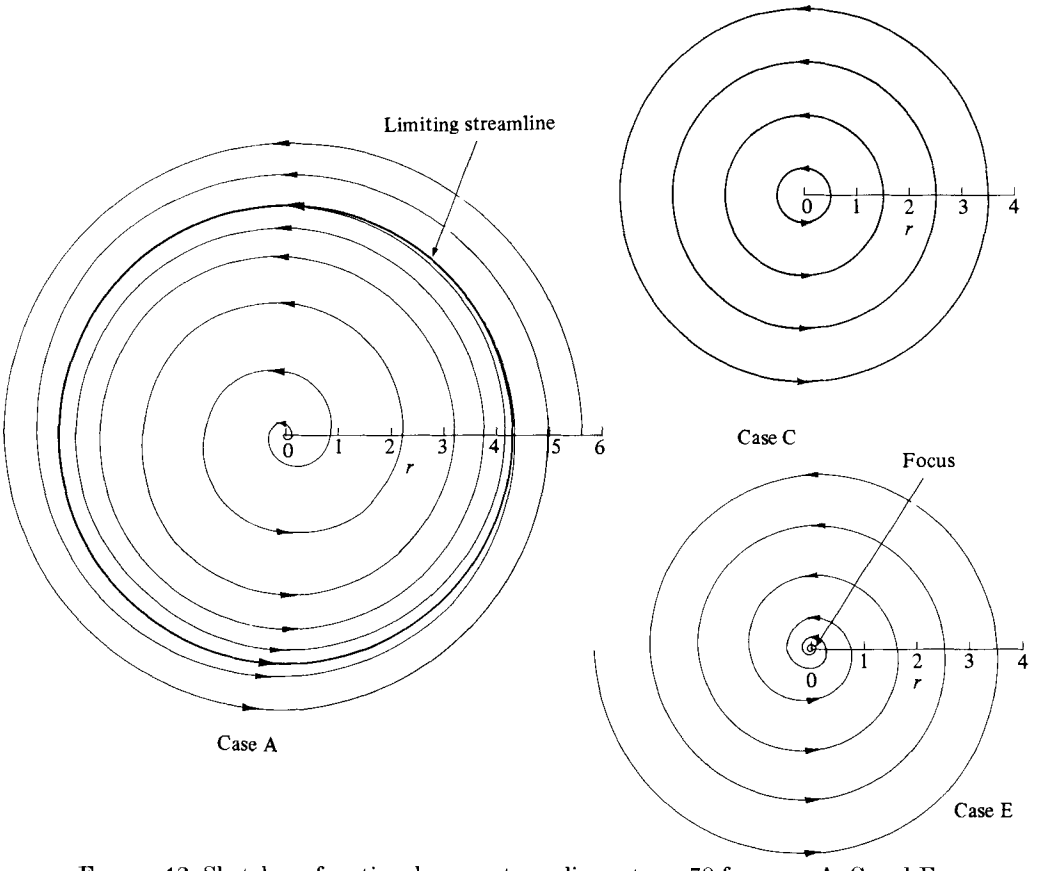


FIGURE 12. Sketches of sectional mean streamlines at $z = 78$ for cases A, C and E. Note that the azimuthal ordinate is not to scale.

momentum in the region $r < r_1$. We have this situation in case A (figure 12), where a limiting streamline is seen to separate the inward-spiralling outer streamline (stretching) from the outward-spiralling inner one (compression). Note that a similar trajectory pattern is to be expected during overcirculation, which may be induced by a growth rate in excess of $(\nu t)^{\frac{1}{2}}$; and which, in view of the above discussion, would seem more likely in the presence of a jet rather than a wake.

The details of the spiral depend to a large extent upon the radial velocity, which we should now like to discuss. $v_r$ is very much smaller than $v_z$ (compare figures 3 and 11), and is usually ignored in the analysis of a trailing vortex whenever $|v_z - 1| \ll 1$. This does not mean that $v_r$ is zero (for we can evaluate it from (4) once $\partial v_z/\partial z$ is known from (3)) and that the mean sectional streamlines are circles, but that its contribution to vortex growth is likely to be minor. The problem is then somewhat simplified, because the inertia terms in (2) and (3) are linear – at least to leading order – and the ensuing analysis tractable; see for example Moore & Saffman's (1973) analysis of a laminar trailing vortex or Phillips' (1981) analysis of a turbulent one. Uberoi (1977), however, asserts that such an approximation is invalid, and, as we have seen in §4.5 for cases A and E, it is. But are there situations when the assumption is valid, particularly for the vortices trailing from a Jumbo jet?

If the characteristic magnitudes of the variables in a slice of trailing vortex distant

$Z$ from its virtual origin, and of radius $R$ (suitably defined), are $V_r$, $V_z$ and $\Gamma_0$ for $v_r, v_z$ and $\Gamma$ respectively, then from (6)

$$\frac{F}{\Gamma_0^2} \sim \frac{2\pi V_z(V_z-1)R^2}{\Gamma_0^2} - \frac{1}{4\pi},$$

and by making use of (4)

$$V_r \sim \frac{\Gamma_0^2}{2\pi V_z ZR}\left[\frac{F}{\Gamma_0^2}+\frac{1}{4\pi}\right].$$

So that for a line vortex $F/\Gamma_0^2 \sim -1/4\pi$ and $V_r \equiv 0$. Now linear theory is valid provided that $V_r \sim 0$, which requires $F/\Gamma_0^2 \not> O(1/4\pi)$, and cases B–D all satisfy $F/\Gamma_0^2 \not> O(1/4\pi)$, as do the flight data of Verstynen & Dunham (1973) from a C5A Jumbo jet and, as near as can be ascertained, the data of McCormick *et al.* (1968) from Cherokee and Army 0–1 light aircraft. Once $F/\Gamma_0^2 > O(1/4\pi)$, however, the radial velocity may not be ignored and linear theory will no longer provide an adequate description of the vortex. Singh's (1974) data (for which $F/\Gamma_0^2 \approx 8$), which Uberoi cites, and cases A and E are in this category, which may be of relevance to aircraft in the takeoff and landing phase if $\Gamma_0 < 1$.

It is a pleasure to acknowledge Professor B. G. Newman for his many helpful comments and suggestions throughout the course of this experiment, and for supporting both it and the authors from his Defence Research Board (9601–15) and National Research Council of Canada (A7096) grants. We should also like to thank Louis Vrooman (of the Engineering Department's DATAC Computer Laboratory) for his valuable technical support, and Dr A. E. Perry of Melbourne University for several valuable suggestions.

## REFERENCES

BAKER, G. R., BARKER, S. J., BOFAH, K. K. & SAFFMAN, P. G. 1974 *J. Fluid Mech.* **65**, 325–336.

BARKER, G. I. & CROW, S. 1977 *J. Fluid Mech.* **82**, 659–671.

BATCHELOR, G. K. 1964 *J. Fluid Mech.* **20**, 645–658.

CHAMPAGNE, F. H. & SLEICHER, C. A. 1967 *J. Fluid Mech.* **28**, 177–182.

CORSIGLIA, V. R. & DUNHAM, E. R. 1976 *NASA SP* 409.

GOVINDARAJU, S. P. & SAFFMAN, P. G. 1971 *Phys. Fluids* **14**, 2074–2080.

GRAHAM, J. A. H., NEWMAN, B. G. & PHILLIPS, W. R. C. 1974 In *Proc. 9th Congr. Intl Counc. Aero. Sci.*, no. 74-40.

GRAHAM, J. A. H., PHILLIPS, W. R. C. 1975 *McGill Univ. MERL TN* 75–1.

GUITTON, D. E. 1968 *McGill Univ. MERL TR* 68–6.

HOFFMANN, E. R. & JOUBERT, P. N. 1963 *J. Fluid Mech.* **16**, 395–411.

IRWIN, H. P. A. H. 1972 *McGill Univ. MERL TN* 72-1.

LONG, R. R. 1961 *J. Fluid Mech.* **11**, 611–626.

LEIBOVICH, S. & STEWARTSON, K. 1983 *J. Fluid Mech.* **126**, 335–356.

MASON, W. H. & MARCHMAN, J. F. 1972 *NASA CR* 62078.

MCCORMICK, B. W., TANGLER, J. L. & SHERRIEB, H. E. 1968 *J. Aircraft* **5**, 260–267.

MOORE, D. W. & SAFFMAN, P. G. 1973 *Proc. R. Soc. Lond.* A **333**, 491–508.

MORSE, A. 1979 Ph.D. thesis, University of London.

MORTON, B. R. 1969 *J. Fluid Mech.* **38**, 315–333.

PERRY, A. E., LIM, T. T. & CHONG, M. S. 1980 *J. Fluid Mech.* **101**, 243–256.

PHILLIPS, W. R. C. 1981 *J. Fluid Mech.* **105**, 451–467.

PHILLIPS, W. R. C. 1984 *J. Phys.* E: *Sci. Instrum.* (submitted).
POPPLETON, E. D. 1971*a* *J. Aircraft* **8**, 672–673.
POPPLETON, E. D. 1971*b* *McGill Univ. MERL TN* 71–1.
PRATTE, B. D. & KEFFER, J. F. 1972 *Trans. ASME* D: *J. Basic Engng* **94**, 739–748.
PULLIN, D. I. & PHILLIPS, W. R. C. 1981 *J. Fluid Mech.* **104**, 45–53.
RIBEIRO, M. M. & WHITELAW, J. H. 1980 *Proc. R. Soc. Lond.* A **370**, 281–301.
SINGH, P. I. 1974 Doctoral dissertation, University of Colorado, Boulder.
SMITH, H. C. 1980 *J. Aircraft* **17**, 861–866.
SMITH, P. A. 1973 Doctoral dissertation, McGill University.
TOWNSEND, A. A. 1976 *The Structure of Turbulent Shear Flow.* Cambridge University Press.
UBEROI, M. S. 1977 *Phys. Fluids* **20**, 1785.
VERSTYNEN, H. A. & DUNHAM, R. E. 1973 *NASA TN* D-7172.
VOGEL, W. M. 1968 *McGill Univ. MERL TN* 68-1.
WYGNANSKI, I. & FIEDLER, H. E. 1969 *J. Fluid Mech.* **38**, 577–612.